Materials Science-Poland, 32(2), 2014, pp. 236-242
http://www.materialsscience.pwr.wroc.pl/
DOI: 10.2478/s13536-013-0177-6

VERSITA

Synthesis of V_2O_3/C composites with different morphologies by a facile route and phase transition properties of the compounds

YIFU ZHANG[1], NANNAN WANG[1], YUTING HUANG[1], CHI HUANG[2], XIAO MEI[3], CHANGGONG MENG[1]*

[1]School of Chemistry, Dalian University of Technology, Dalian 116024, PR China
[2]College of Chemistry and Molecular Sciences, Wuhan University, Wuhan 430072, PR China
[3]School of Resources and Environmental Science, Wuhan University, Wuhan, 430079, PR China

V_2O_3 and amorphous carbon composites (V_2O_3/C composites) with different morphologies (e.g. nanospheres, nanorods and nanosheets) were, for the first time, successfully synthesized by a facile hydrothermal route and subsequent calcination. The as-obtained samples were characterized by X-ray powder diffraction (XRD), energy dispersive spectrometery (EDS), elemental analysis (EA), Fourier transform infrared spectroscopy (FT-IR), Raman spectroscopy, scanning electron microscopy (SEM) and transmission electron microscopy (TEM). The morphology of V_2O_3/C composites could be easily controlled by varying the reaction time, and, as a result, V_2O_3/C composites with nanospheres, nanorods and nanosheets were selectively synthesized. Furthermore, the phase transition property of V_2O_3/C composites was measured by differential scanning calorimetry (DSC), suggesting that V_2O_3/C composites exhibit the phase transition similar to V_2O_3, which could expand the potential applications of materials related to V_2O_3 in the future.

Keywords: *nanostructures; V_2O_3 amorphous carbon composites; chemical synthesis; phase transitions*

1. Introduction

In recent years, vanadium oxides and their derived compounds have attracted increasing attention as the functional materials because of their layered structures and specific chemical and physical properties, which make them attractive for a wide range of practical and potential applications, such as catalysts, cathode materials for reversible lithium-ion batteries, gas sensors, intelligent thermochromic windows, optical switching devices, laser shield, optical or electrical modulators and so on [1–16]. The family of vanadium oxides, V_2O_3 exhibits a metal-to-insulator transition (MIT) as a function of temperature, doping concentration or pressure [17–20]. It shows a first-order phase transformation from a monoclinic antiferromagnetic insulator (AFI) to a rhombohedral paramagnetic metal (PM) near 150 K, with a jump in the resistivity of about seven orders of magnitude. A broad second-order transformation occurs at about 350 K to about 550 K from a PM phase to a second metal (PM') phase [19, 21, 22]. These feature properties make V_2O_3 and its derivative compounds to have wide practical applications, such as optical devices, temperature sensors, field effect transistors, conductive composite polymer, catalyst and so on [19, 23–26].

In the previous decades, the fabrication of V_2O_3 was mainly focused on bulk powders and spherical particles [23, 27–32]. Recently, some techniques for preparing V_2O_3 with a novel morphology have been reported. V_2O_3 nanorods were converted from VO_2(B) nanorods by reducing in 5 % H_2: 95 % N_2 [33]. V_2O_3 porous urchin-like micro-nanostructures were synthesized by a simple top-down strategy of pyrolyzing a vanadyl ethylene glycolated precursor [34]. Dandelion-like V_2O_3 microspheres with core-shell structures were reported by Su [35]. It was reported that the prop-

*E-mail: cgmeng@dlut.edu.cn

erties of the materials and devices were greatly influenced by the powder particle characteristics such as particle size, particle size distribution and morphology as well as powder surface chemistry and their preparation methods [23]. Thus, the synthesis of V_2O_3 with novel morphologies is still a challenge for materials scientists. Herein, we report the fabrication of V_2O_3 with different morphologies: nanospheres, nanorods and nanosheets.

Very recently, some hybrid materials related to V_2O_3 have been studied. Carbon-coated V_2O_3 was prepared using $VO(OC_2H_5)_3$ via the reaction under autogenic pressure at elevated temperature [36]. Highly ordered lamellar V_2O_3-based hybrid nanorods were synthesized using $VOCl_3$ and phenethyl alcohol as starting materials by the solvothermal route [37]. V_2O_3@carbon nanobelts were fabricated by thermal treatment of $V_3O_7{\cdot}H_2O$@C [38] or VO_2(B)@C [39, 40] in three steps: (1) synthesis of $V_3O_7{\cdot}H_2O$ or VO_2(B); (2) coating carbon on the surface of $V_3O_7{\cdot}H_2O$ or VO_2(B); (3) heating treatment of $V_3O_7{\cdot}$ H_2O@C or VO_2(B)@C in an inert atmosphere. Except those, there are few literature reports on V_2O_3 hybrid materials. It is apparent that the routes for their fabrication are of low efficiency and high cost. Therefore, it is urgently necessary to find a facile route to synthesize V_2O_3 hybrid materials.

In this study, V_2O_3/C composites with different morphologies were obtained by a facile hydrothermal route and subsequent calcination. This route is very simple, economical and practical for industrial applications. What's more, different morphologies (e.g. nanospheres, nanorods and nanosheets) of V_2O_3/C composites can be selectively prepared by controlling the synthetic conditions in this system. The as-obtained V_2O_3@C composite exhibits the same phase transition property as V_2O_3, which could expand the possible applications of materials related to V_2O_3 in the future.

2. Experimental section

2.1. Synthetic route

Vanadium pentoxide (V_2O_5), ethanol, and D–(+)–Glucose ($C_6H_{12}O_6{\cdot}H_2O$) with analytical grade were purchased from Sinopharm Chemical Reagent Co., Ltd. and used without any further purification. The synthesis of V_2O_3/C composites mainly included two steps: (1) 0.15 g of bulk V_2O_5 powder and 0.27 g of $C_6H_{12}O_6{\cdot}H_2O$ were dispersed into 30 mL of deionized water, and then the mixture was vigorously stirred for 1 h with a magnetic stirrer at the room temperature. After the solution became a suspension, it was transferred into a 40 mL Teflon lined stainless steel autoclave, which was sealed and maintained at 180 °C for 3 – 96 h (the reaction time controlled the morphology of V_2O_3/C composites). When the autoclave was cooled to room temperature naturally, the products were filtered off, washed with distilled water and absolute ethanol several times to remove any possible residues, and dried in vacuum at 75 °C for future application. (2) The above precursors were heated in a tube furnace with 5 °C/min heating rate under a flow of argon gas at 700 °C for 2 h, and cooled to room temperature in the argon flow to prevent oxidation of V_2O_3/C composites.

2.2. Characterization

X-ray powder diffraction (XRD) was carried out on D8 X-ray diffractometer equipped with Cu$K\alpha$ radiation, $\lambda = 1.54060$ Å. The morphology and dimensions of the products were observed by scanning electron microscopy (SEM, Quanta 200) and transmission electron microscopy (TEM, JEM-2100). The selected area electron diffraction (SAED) and high resolution transmission electron microscopy (HRTEM) were also carried out with JEM-2100. The sample was dispersed in absolute ethanol and was ultrasonicated before TEM, SAED and HRTEM examinations. The elemental analysis (EA) of the samples was carried out using a Vario EL III equipment (Germany) with a TCD detector to analyze the elements of C, H and N. The chemical composition of as-obtained samples was revealed by use of an energy-dispersive X-ray spectrometer (EDX) attached to a scanning electron microscope (SEM; Quanta 200). The Raman spectrum was taken on a RM-1000 spectrometer (Confocal Raman Microspectroscopy) with an argon-ion laser at an excitation wavelength of 514.5 nm.

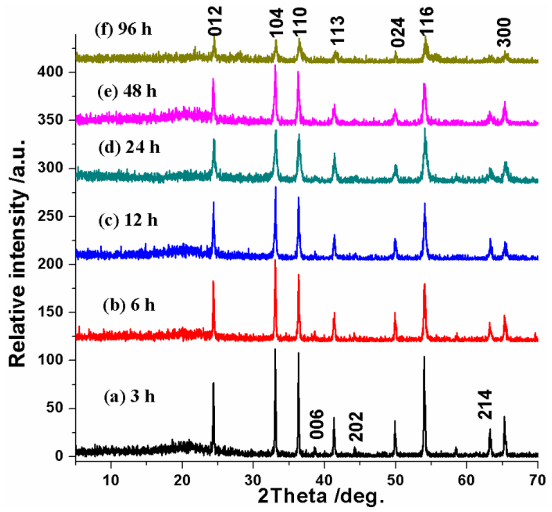

Fig. 1. XRD patterns of the samples obtained at different reaction times: (a) 3 h; (b) 6 h; (c) 12 h; (d) 24 h; (e) 48 h; (f) 96 h.

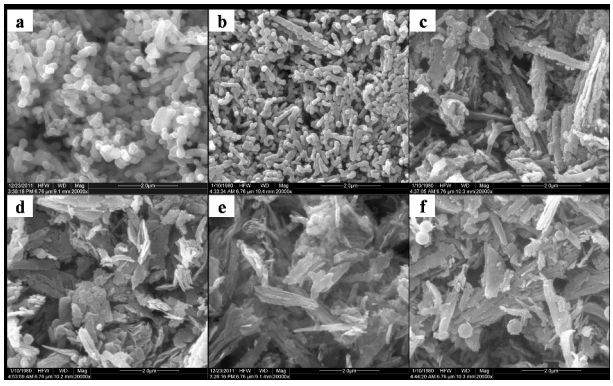

Fig. 2. SEM images of the samples obtained at different reaction times: (a) 3 h; (b) 6 h; (c) 12 h; (d) 24 h; (e) 48 h; (f) 96 h.

Fourier transform infrared spectroscopy (FT-IR) pattern of the solid sample was measured using KBr pellet technique and recorded on a Nicolet 60-SXB spectrometer from 4000 to 400 cm^{-1} with a resolution of 4 cm^{-1}. The phase transition temperature (T_c) of the sample was measured by DSC (DSC822^e, METTLER TOLEDO) with 5 °C/min heating rate.

3. Results and discussion

In our experiments, it was found that the reaction time had a great influence on the crystalline phase and morphology of the final samples. Keeping other parameters unchanged, only the synthetic time was varied at definite periods of 3, 6, 12, 24, 48 and 96 h. The as-obtained products were separately characterized by XRD and SEM, as shown in Fig. 1 and 2, respectively.

All the peaks from Fig. 1 can be indexed to the rhombohedral crystalline phase of V_2O_3 (JCPDS No. 71-280) [41]. No impurity phases, such as V_2O_5, V_3O_7, V_6O_{13}, VO_2(B) and VO_2(M), have been detected, revealing the as-obtained crystalline V_2O_3 with high purity. Besides, we can also see the disordered background and a broadened peak ranging from 15° to 25°, which indicates that some non-crystalline materials have probably remained in the sample. According to the starting materials, the non-crystalline materials can be amorphous carbon, which will be verified in detail in the following discussion.

Fig. 2 shows the SEM images of the samples, which disclose that the morphologies of the samples are very different. When the reaction was carried out for 3 h (Fig. 2a), the sample morphology was basically composed of nanospheres and short nanorods. With extending the reaction time to 6 h, short nanorods have been obtained (Fig. 2b). After 12 h, larger nanorods have been formed (Fig. 2c). The nanorods tend to aggregate due to their surface, containing some active functional groups, which has been proven by FT-IR spectrum. However, with increasing the reaction time to 24, 48 or 96 h, the as-obtained samples exhibited similar morphologies. As depicted in Fig. 2d – 2f, the products are composed of nanosheets.

To get a further insight into the morphologies and structures of the as-obtained samples, some corresponding TEM tests were carried out, as shown in Fig. 3. For the reaction time of 3 h, the morphology of the sample consists of nanospheres and short nanorods (Fig. 3a – 3c), which well agrees with the SEM observation (Fig. 2a). The polycrystalline SAED (inset in Fig. 3a) shows V_2O_3 to be well crystallized, and the high magnification TEM reveals that the sample has two kinds of structures (inset in Fig. 3b and 3c). After 48 h, as depicted in Fig. 3d, nanosheets are obtained.

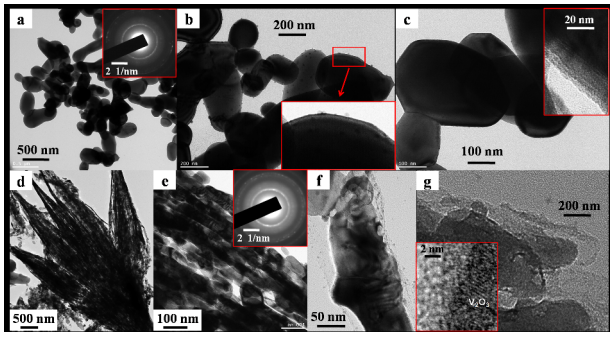

Fig. 3. TEM images of the samples obtained at different reaction times: (a – c) 3 h; (d – g) 48 h.

However, the TEM images (Fig. 3d – 3g) reveal that these nanosheets consist of nanobelts (Fig. 3e). These results indicate that the nanobelts are aggregated to form nanosheets after 24 h, in agreement with the SEM observations (Fig. 2d – 2f). The polycrystalline SAED (inset in Fig. 3e) also shows V_2O_3 to be well crystallized, and the HRTEM images in Fig. 3g reveal that the as-obtained sample has two kinds of phases, too.

Based on the above analyses, both XRD and TEM tests reveal that the as-obtained samples have two kinds of phases: one is the crystalline V_2O_3, the other is amorphous material. To verify the composition of the amorphous material, some corresponding measurements including EDS, EA, FT-IR and Raman were carried out.

Fig. 4a shows a typical EDS spectrum of the as-obtained composite, which presents the composition of the sample surface, revealing that the as-synthesized sample consists only of C, O and V elements. The typical elemental analysis (EA) of the as-obtained sample shows that it contains 6.526 wt.% of C and 0.556 wt.% of H, revealing that it probably contains some organic functional groups, which is further confirmed by FT-IR (Fig. 4b). The peaks at 2950 – 2850 cm^{-1} and 1048 cm^{-1} are the characteristic C–H stretches, which will facilitate the linkage of catalytic species or polymers to the surface in its potential applications [38, 42–44]. The peak at 980 cm^{-1} corresponds to the symmetric stretching of the $\nu_s(V^{3+}{=}O)$ bond [45], in agreement with the XRD observation. Besides, the absorptions at 3440, 1632 and 1384 cm^{-1} are due to water and nitrate adsorbed on the KBr and can be disregarded [46]. All the products have similar FT-IR spectra to Fig. 4b, revealing that all the products have similar compositions. Fig. 4c shows a typical Raman spectrum of the as-obtained composite, which exhibits two peaks located at 1353 cm^{-1} (D-band) and 1598 cm^{-1} (G-band). These two peaks are characteristic of amorphous carbon [36, 42, 47]. It was reported [43, 48, 49] that the peak at 1353 cm^{-1} is usually associated with the vibrations of carbon atoms with dangling bonds for the in-plane terminations of disordered graphite, labeled as the D-band, and the peak at 1598 cm^{-1} is closely related to the vibration in all sp^2-bonded carbon atoms in a two-dimensional hexagonal lattice, such as in a graphite layer, labeled as the G-band (corresponding to the E_{2g} mode). The intensity ratio of the G- and D-bands is $I_G/I_D = 1.27$ for the sample. The relatively high intensity of the D-peak proves that the coating comprises disordered carbon. On the basis of the above analyses it can be inferred that the as-obtained sample consists of crystalline V_2O_3 and amorphous carbon (described as V_2O_3/C composites).

From the SEM and TEM images it can be concluded that V_2O_3/C composites with different morphologies were successfully synthesized by our current synthetic route. According to this synthetic route, organic carbon coated VO_x core-shell structured nanobelts were first formed [50]. Subsequently, V_2O_3/C composites were prepared at 700 °C for 2 h under the Ar atmosphere. On one hand, it was reported that glucose can be carbonized to form carbon spheres [51] or amorphous carbon can be coated on the surface of metal oxides [42–44]. The carbonization step may arise from cross-linking induced by intermolecular dehydration of linear or branchlike oligosaccharides or other macromolecules [51]. However, the carbon spheres or amorphous carbon cannot be formed when the concentration of glucose is lower than 0.5 M. In our route, the concentration of glucose was only about 0.045 M. Therefore, the amorphous carbon could not be formed and only some oligosaccharides and macromolecules, which could be adsorbed on the surface of vana-

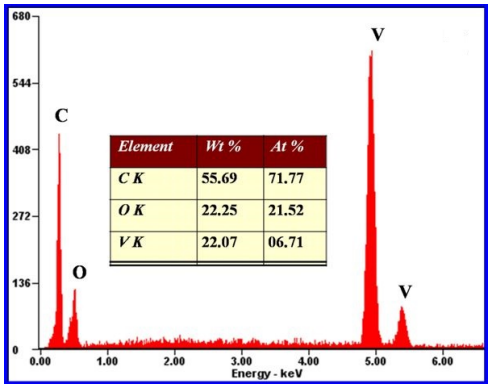

(a)

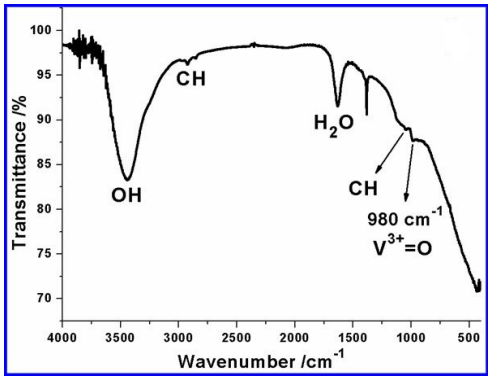

(b)

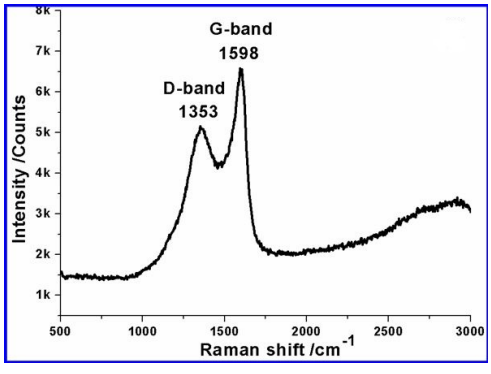

(c)

Fig. 4. The typical spectra of the as-obtained samples: (a) EDS; (b) FT-IR; (c) Raman.

dium oxides, were probably formed. On the other hand, V_2O_5 can be reduced to low-valence vanadium oxides in the presence of glucose due to its inherent reductibility [52]. The oligosaccharides or macromolecules can be adsorbed on the surface of low-valance vanadium oxides nanostructures because of their large specific surface area. Therefore, organic carbon coated VO_x core-shell structured nanobelts are first synthesized, forming the precursors for the synthesis of V_2O_3/C composites. It has been reported that the active carbon can react with high-valence vanadium oxides to form low-valence vanadium oxides [38, 40, 49, 53]. In our studies, V_2O_3/C composites have been obtained by thermal treatment with organic carbon coated VO_x core-shell structured nanobelts at 700 °C for 2 h under the inert atmosphere. The chemical reaction can be expressed as follows:

$$VO_x + C \rightarrow V_2O_3 + CO \qquad (1)$$

The residual carbon remains to form amorphous carbon which finally forms the V_2O_3/C composites.

When the phase transition of V_2O_3 occurs, it exhibits a noticeable endothermal and exothermal profile in the heating and cooling DSC curves, which corresponds to the phase transition of V_2O_3. In this paper, the phase transition of V_2O_3/C composites was investigated by DSC, as shown in Fig. 5. The T_c of V_2O_3/C is about −109 °C in the heating cycle, while it is about −131 °C in the cooling cycle. The result reveals that V_2O_3/C composites exhibit the same phase transition property as pure V_2O_3, which can expand the applications of materials related with V_2O_3 in the future. The heating and cooling curves obtained for different cycles are basically coincided, which indicates that the phase transition of V_2O_3/C has good reversibility.

4. Conclusion

In conclusion, V_2O_3/C composites with different morphologies, including nanospheres, nanorods and nanosheets were successfully synthesized, for the first time, by a facile hydrothermal route and subsequent calcination at 700 °C for 2 h. The as-obtained V_2O_3/C composites were characterized by XRD, EDS, EA, FT-IR, Raman, SEM and TEM tests. The carbon in the V_2O_3/C composites was amorphous. The morphology of V_2O_3/C can be easily controlled by the reaction time. Furthermore, V_2O_3/C composite exhibited

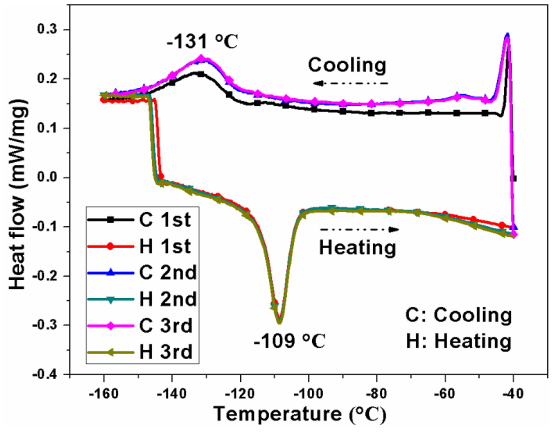

Fig. 5. Typical DSC curves of V_2O_3/C composites after three cycles.

the same phase transition property as pure V_2O_3, which can expand the applications of materials related to V_2O_3 in the future.

Acknowledgements

This work was partially supported by the National Natural Science Foundation of China (Grant No. 21271037), the Fundamental Research Funds for the Central Universities and China Postdoctoral Science Foundation funded project.

References

[1] QI J., NING G., HUA R., TIAN M., LIU S., *Mater. Sci.-Poland*, 30 (2012), 151.
[2] ZHANG Y., HUANG Y., ZHANG J., WU W., NIU F., ZHONG Y., LIU X., LIU X., HUANG C., *Mater. Res. Bull.*, 47 (2012), 1978.
[3] ZHANG Y., FAN M., LIU X., XIE G., LI H., HUANG C., *Solid State Commun.*, 152 (2012), 253.
[4] ZHANG Y., LI W., FAN M., ZHANG F., ZHANG J., LIU X., ZHANG H., HUANG C., LI H., *J. Alloy. Compd.*, 544 (2012), 30.
[5] SURNEV S., RAMSEY M.G., NETZER F.P., *Prog. Surf. Sci.*, 73 (2003), 117.
[6] ZHANG Y., ZHANG J., FAN M., LONG Y.A., ZHONG Y., LIU X., HUANG C.H.I., *B. Mater. Sci.*, 36 (2013), 345.
[7] ZHANG Y., CHEN C., WU W., NIU F., LIU X., ZHONG Y., CAO Y., LIU X., HUANG C., *Ceram. Int.*, 39 (2013), 129.
[8] LIU J., WANG X., PENG Q., LI Y., *Adv. Mater.*, 17 (2005), 764.
[9] ZHANG Y., ZHANG J., ZHANG X., HUANG C., ZHONG Y., DENG Y., *Mater. Lett.*, 92 (2013), 61.
[10] ZHANG Y., ZHANG J., ZHANG X., DENG Y., ZHONG Y., HUANG C., LIU X., LIU X., MO S., *Ceram. Int.*, 39 (2013), 8363.
[11] PARKIN I.P., MANNING T.D., *J. Chem. Educ.*, 83 (2006), 393.
[12] ZHANG Y., ZHANG J., ZHANG X., MO S., WU W., NIU F., ZHONG Y., LIU X., HUANG C., LIU X., *J. Alloy. Compd.*, 570 (2013), 104.
[13] ZHANG Y., FAN M., NIU F., WU W., HUANG C., LIU X., LI H., LIU X., *Curr. Appl. Phys.*, 12 (2012), 875.
[14] XU L., ZHANG Y., DENG Y., ZHONG Y., MO S., CHENG G., HUANG C., *Mater. Res. Bull.*, 48 (2013), 3620.
[15] ZHANG Y., LIU X., XIE G., YU L., YI S., HU M., HUANG C., *Mater. Sci. Eng. B-Adv.*, 175 (2010), 164.
[16] ZHANG Y., FAN M., NIU F., ZHONG Y., HUANG C., LIU X., WANG B., LI H., *Micro Nano Lett.*, 6 (2011), 888.
[17] FOEX M., *CR Chim.*, 223 (1946), 1126.
[18] MCWHAN D.B., REMEIKA J.P., *Phys. Rev. B*, 2 (1970), 3734.
[19] HENDRIX B.C., WANG X., CHEN W., CUI W.Q., *J. Mater. Sci.*, 3 (1992), 113.
[20] SEIKH M.M., NARAYANA C., SOOD A.K., MURUGAVEL P., KIM M.W., METCALF P.A., HONIG J.M., RAO C.N.R., *Solid State Commun.*, 138 (2006).
[21] KOKABI H.R., RAPEAUX M., AYMAMI J.A., DESGARDIN G., *Mater. Sci. Eng. B-Adv.*, 38 (1996), 80.
[22] DERNIER P.D., MAREZIO M., *Phys. Rev. B*, 2 (1970), 3771.
[23] ZHENG C.M., ZHANG X.M., HE S., FU Q., LEI D.M., *J. Solid State Chem.*, 170 (2003), 221.
[24] BALLARINI N., BATTISTI A., CAVANI F., CERICOLA A., LUCARELLI C., RACIOPPI S., ARPENTINIER P., *Catal. Today*, 116 (2006), 313.
[25] PAN Y., WU G.Z., YI X.S., *J. Mater. Sci.*, 29 (1994), 5757.
[26] ZHANG Y., ZHANG J., NIE J., ZHONG Y., LIU X., HUANG C., *Micro Nano Lett.*, 7 (2012), 782.
[27] PINNA N., ANTONIETTI M., NIEDERBERGER M., *Colloid. Surface. A*, 250 (2004), 211.
[28] ZHANG K.F., SUN X.Z., LOUU G.W., LIU X., LI H.L., SU Z.X., *Mater. Lett.*, 59 (2005), 2729.
[29] RAMANA C.V., UTSUNOMIYA S., EWING R.C., BECKER U., *Solid State Commun.*, 137 (2006), 645.
[30] SEDIRI F., GHARBI N., *Mater. Sci. Eng. B-Adv.*, 123 (2005), 136.
[31] TEGHIL R., D'ALESSIO L., DE BONIS A., GALASSO A., IBRIS N., SALVI A.M., SANTAGATA A., VILLANI P., *J. Phys. Chem. A*, 113 (2009), 14969.
[32] LIU X.H., ZHANG Y.F., YI S.P., HUANG C., LIAO J., LI H.B., XIAO D., TAO H.Y., *J. Supercrit. Fluid.*, 56 (2011), 194.
[33] CORR S.A., GROSSMAN M., SHI Y.F., HEIER K.R., STUCKY G.D., SESHADRI R., *J. Mater. Chem.*, 19 (2009), 4362.
[34] XU Y., ZHENG L., WU C., QI F., XIE Y., *Chem.-Eur. J.*, 17 (2011), 384.
[35] CHEN J.A., LIU X.A., SU Z.X., *Micro Nano Lett.*, 6 (2011), 102.
[36] ODANI A., POL V.G., POL S.V., KOLTYPIN M.,

GEDANKEN A., AURBACH D., *Adv. Mater*., 18 (2006), 1431.

[37] SUN Y.F., JIANG S.S., BI W.T., WU C.Z., XIE Y., *J. Power Sources*, 196 (2011), 8644.

[38] ZHANG Y., FAN M., LIU X., HUANG C., LI H., *Eur. J. Inorg. Chem*., 2012 (2012), 1650.

[39] ZHANG Y., ZHANG F., YU L., FAN M., ZHONG Y., LIU X., MAO Y., HUANG C., *Colloid. Surface. A*, 396 (2012), 144.

[40] ZHANG Y., FAN M., HU L., WU W., ZHANG J., LIU X., ZHONG Y., HUANG C., *Appl. Surf. Sci*., 258 (2012), 9660.

[41] RICE C.E., ROBINSON W.R., *J. Solid State Chem*., 21 (1977), 145.

[42] ZHANG Y., LIU X., CHEN D., YU L., NIE J., YI S., LI H., HUANG C., *J. Alloy. Compd*., 509 (2011), L69.

[43] ZHANG Y., LIU X., NEI J., YU L., ZHONG Y., HUANG C., *J. Solid State Chem*., 184 (2011), 387.

[44] ZHANG Y., ZHOU M., FAN M., HUANG C., CHEN C., CAO Y., LI H., LIU X., *Curr. Appl. Phys*., 11 (2011), 1159.

[45] GILSON T.R., BIZRI O.F., CHEETHAM N., *Dalton T*., (1973), 291.

[46] ROS T.G., VAN DILLEN A.J., GEUS J.W., KONINGSBERGER D.C., *Chem.-Eur. J*., 8 (2002), 1151.

[47] LLIE A., DURKAN C., MILNE W.I., WELLAND M.E., *Phys. Rev. B*, 66 (2002), 045412/1.

[48] DRESSELHAUS M.S., DRESSELHAUS G., EKLUND M.A.P., *Raman Scattering in Carbon Materials*, in: PELLETIER M.J. (Ed.), *Analytical Application of Raman Spectroscopy*, Wiley-Blackwell Publishing, Oxford, 1999, p. 367.

[49] ZHANG Y., FAN M., WU W., HU L., ZHANG J., MAO Y., HUANG C., LIU X., *Mater. Lett.*, 71 (2012), 127.

[50] ZHANG Y., ZHANG J., ZHONG Y., YU L., DENG Y., HUANG C., LIU X., *Appl. Surf. Sci*., 263 (2012), 124.

[51] SUN X., LI Y., *Angew. Chem. Int. Edit*., 43 (2004), 597.

[52] ZHANG Y., FAN M., ZHOU M., HUANG C., CHEN C., CAO Y., XIE G., LI H., LIU X., *B. Mater. Sci*., 35 (2012), 369.

[53] ZHANG Y., CHEN C., ZHANG J., HU L., WU W., ZHONG Y., CAO Y., LIU X., HUANG C., *Curr. Appl. Phys*., 13 (2013), 47.

Received 2013-07-19
Accepted 2014-02-05